Available online at www.sciencedirect.com
ScienceDirect
Geochimica et Cosmochimica Acta 71 (2007) 5180–5190
Geochimica et Cosmochimica Acta
www.elsevier.com/locate/gca

An atomic level study of rhenium and radiogenic osmium in molybdenite

Yoshio Takahashi [a,b,*], Tomoya Uruga [c], Katsuhiko Suzuki [d], Hajime Tanida [c], Yasuko Terada [c], Keiko H. Hattori [e]

[a] *Department of Earth and Planetary Systems Science, Graduate School of Science, Hiroshima University, Higashi-Hiroshima, Hiroshima 739-8526, Japan*
[b] *Laboratory for Multiple Isotope Research for Astro- and Geochemical Evolution (MIRAGE), Hiroshima University, Hiroshima 739-8526, Japan*
[c] *SPring-8, Japan Synchrotron Radiation Research Institute (JASRI), Sayo-cho, Hyogo 679-5198, Japan*
[d] *Institute for Research on Earth Evolution (IFREE), Japan Agency for Marine-Earth Science and Technology (JAMSTEC), Yokosuka 237-0061, Japan*
[e] *Department of Earth Sciences, University of Ottawa, Ottawa, Ont., Canada K1N 6N5*

Received 28 December 2006; accepted in revised form 3 August 2007; available online 7 September 2007

Abstract

Local atomic structures of Re and radiogenic Os in molybdenite from the Onganja mine, Namibia, were examined using X-ray absorption fine structure (XAFS). Rhenium L_{III}-edge X-ray absorption near-edge structure (XANES) and extended X-ray absorption fine structure (EXAFS) show that the oxidation state of Re, the interatomic distances between Re and the neighboring atoms, and the coordination number of Re to S are very similar to those of Mo in molybdenite. The results confirm that Re is present as Re(IV) in the Mo site in molybdenite.

Measurement of L_{III}-edge XANES and EXAFS of a minor concentration (8.55 ppm) of radiogenic Os was accomplished in fluorescence mode by removing the interfering X-rays from Re and other elements using a crystal analyzer system. The data indicate that the oxidation state of radiogenic Os is Os(III) and Os(IV) and clearly different from Os(II) in natural sulfide minerals, such as OsS_2 (erlichmanite). XANES data also suggest that radiogenic Os does not form a secondary Os phase, such as OsS_2 or Os metal, in molybdenite.

EXAFS of radiogenic Os was successfully simulated assuming that Os is present in the Mo site in molybdenite. The data are consistent with the XANES data; Os does not form Os phases in molybdenite. The EXAFS simulation showed that the interatomic distance between Os and S is 2.27 Å, which is 0.12 Å smaller than the distances of Re–S and Mo–S (2.39 Å) in molybdenite. Similar valences and ionic sizes of Re and Mo in molybdenite support the fact that large amounts of Re can be incorporated into the Mo site as has been observed in previous studies, whereas the different properties of Os compared to Mo and Re suggested here support much lower abundance of common Os in molybdenite. This makes molybdenite an ideal mineral for the Re–Os geochronometer as shown in many studies. However, the shorter distance between radiogenic Os and S compared to those of Re–S and Mo–S in molybdenite suggests that the radiogenic Os has a smaller ionic size than Re(IV) and Mo(IV). Furthermore, Os may be partly present as Os(III). Smaller and lower charge Os can diffuse faster than larger and higher charge Re in molybdenite at a given set of conditions. Hence, our study provides an atomic-level explanation for the high mobility of Os compared to Re, which has been suggested by earlier workers using laser ablation ICP-MS.

* Corresponding author. Fax: +81 82 424 0735.
E-mail address: ytakaha@hiroshima-u.ac.jp (Y. Takahashi).

0016-7037/$ - see front matter © 2007 Published by Elsevier Ltd.
doi:10.1016/j.gca.2007.08.007

1. INTRODUCTION

Radiometric dating has been widely applied to various terrestrial and extraterrestrial materials (Faure and Mensing, 2004). Such dating assumes the retention of both parent and daughter isotopes in the samples since formation. The chemical properties of the daughter commonly differ from those of the parent, which may result in their separation. Thus, their retention in the system may depend on the chemical environment of both elements, which determines their stabilities in situations of various processes such as metamorphism, alteration, and diffusion within the crystal. Therefore, the chemical states of parent and daughter isotopes in the mineral or rock samples may be important for precise dating.

Since the first application of the ^{187}Re–^{187}Os system for dating of molybdenite by Herr and Merz (1955), the dating of molybdenite has been established as a robust geochronometer resistant to regional deformation and metamorphism (e.g., Stein et al., 1997, 2001, 2003; Raith and Stein, 2000; Watanabe and Stein, 2000; Selby and Creaser, 2001a,b, 2004). In particular, the method has become an important tool in dating the timing and duration of sulfide mineralization in ore-forming systems (e.g., Suzuki et al., 1996; Stein et al., 1997, 1998). However, decoupling of ^{187}Os and Re possibly due to high mobility of Os relative to Re has been observed within molybdenite crystals by micrometer scale analysis using the laser ablation ICP-MS technique (Stein et al., 2001, 2003; Kosler et al., 2003; Selby and Creaser, 2004). Hence, it has been indicted that successful dating requires careful selection of representative samples from a specific geologic occurrence with a sufficient volume of the sample for the analysis (Stein et al., 2001, 2003; Selby and Creaser, 2004; Stein, 2006). In this study, we examine the local structures of Re and radiogenic ^{187}Os in molybdenite using their X-ray absorption fine structure (XAFS) to evaluate the atomic scale environment for the two elements and the cause of the decoupling. Since the abundance of common Os is negligible in molybdenite (Herr and Merz, 1955; Hirt et al., 1963; Morgan et al., 1968; Stein et al., 2001), the XAFS data of Os in molybdenite provides the information on the decay product, ^{187}Os.

For our study, fluorescence XAFS spectra of Re and Os were employed because they have low detection limits and high selectivity of any trace elements in a variety of samples (e.g., Takahashi et al., 2000, 2004). XAFS consists of two energy regions, X-ray absorption near-edge structure (XANES) and extended X-ray absorption fine structure (EXAFS). We used both sets of data to evaluate the oxidation state and local atomic structure of Re and radiogenic Os. Retrieving the data from trace Os was an analytical challenge because its spectrum was obscured by the intense fluorescence X-ray emitted from Re and other scattering X-rays. This was overcome by employing a crystal analyzer in Laue geometry to extract Os L_α emission (Takahashi et al., 2006).

2. SAMPLES AND METHODS

2.1. Samples and materials

Natural molybdenite (MoS_2; polytype: 2H) was obtained from the Onganja mine in the Damara Facies, 70 km northeast of Windhoek, in central Namibia. The molybdenite was collected from a post-metamorphic quartz–biotite vein in the schist of the Late Proterozoic Kuiseb Formation. The concentrations of Re and Os in the sample measured by inductively coupled plasma-mass spectrometer (ICP-MS) were 1610 ± 10 and 8.55 ± 0.04 ppm, respectively, following the procedures reported in Suzuki et al. (1992). The sample was chosen for this study due to its high concentrations of Re and Os; the greater the concentrations, the more clearly is the XAFS spectrum. The isotopic composition of Os in the Onganja molybdenite shows that 99.2% of Os was ^{187}Os (Schieder et al., 1981), implying that more than 99% of ^{187}Os is a decay product of ^{187}Re.

Reference materials used for Os L_{III}-edge XAFS were Os metal, $Os^{II}S_2$, $Os^{III}Cl_3$, and $Os^{VIII}O_4$ as reported by Sakakibara et al. (2005). Osmium metal and $OsCl_3$ were purchased from Rare Metallic Co. Ltd., whereas OsO_4 is from Kanto Chemical Co. Ltd. Osmium disulfide (OsS_2, erlichmanite) was synthesized by following the procedure reported in Hayashi et al. (2000). Reference materials for Re were Re metal, $Re^{IV}S_2$, $Re^{IV}O_2$, and $Re^{VI}O_3$ obtained from Rare Metallic Co. Ltd. and ReO_4^- solution from Kanto Chemical Co. Ltd. All purchased chemicals were at reagent grades used without further purification for the XAFS measurements.

2.2. XAFS measurements

Rhenium L_{III}-edge XAFS was measured at BL-12C (bending magnet) of the Photon Factory (PF) at High Energy Accelerator Research Organization (KEK), Tsukuba, Japan (Nomura and Koyama, 1996). In the beamline, X-rays from a synchrotron operated at 2.5 GeV (current: 450–300 mA) were monochromatized with a Si(1 1 1) double-crystal monochromator, and focused to an area of 1 (horizontal) $\times$ 0.5 (vertical) mm^2 with a bent cylindrical mirror, which also reduces the higher order. XAFS spectra were obtained in transmission mode for reference materials, and in fluorescence mode for Re in molybdenite. The fluorescence yield was measured using a 19-element Ge semiconductor detector (SSD). The total counts were maintained at less than 200 kcps by adjusting the distance between the SSD and the sample. Counts for high intensities of fluorescence and scattering X-rays are corrected for dead counting time (Nomura, 1998).

Osmium L_{III}-edge XAFS of Os in molybdenite was measured in the fluorescence mode using a crystal analyzer at an undulator beamline, BL37XU, at SPring-8, Japan (Terada et al., 2004). The beamline consists of Si(1 1 1) double-crystal monochromator and Rh-coated mirror for suppression of higher harmonics. The beam size and the monochromatic photon flux at the sample position were 0.2 (horizontal) $\times$ 0.8 (vertical) mm^2 and 4.4×10^{12} photons/s, respectively. The sample was placed at 45° to the incident X-ray beam. The extraction of Os L_α fluorescence used a commercially available fluorescence analyzer (BCLA: Bent Crystal Laue Analyzer) made by Oxford Danfysik (Zhong et al., 1999). The analyzer, DCA 0950, used here was specially designed to determine the intensity

of fluorescence X-rays ranging from 8.5 to 10.5 keV, which covers Os L_α fluorescence X-rays. The analyzer consists of a log spiral Si(1 1 1) crystal and slits made of Mo metal. A 19-element Ge semiconductor detector (Ortec IGLET-X-11160) was used for detection. The detector was well shielded by a Pb sheet to collect X-rays only from the crystal analyzer. XAFS spectra of Os in reference materials were measured in transmission mode.

2.3. XAFS analysis

EXAFS data were analyzed using REX2000 ver.2.3 (Rigaku Co.) with parameters generated by the computer program FEFF7.02 (an automated program for *ab initio* multiple scattering calculations of XAFS; Zavinsky et al., 1995; Ankudinov and Rehr, 1997). Initial structural data for the FEFF calculations were provided by ATOMS (Ravel, 2001) using crystallographic data listed in Table 1. For the simulation of Re in molybdenite, initial structure for the FEFF calculation assumed that Re replaces Mo in the molybdenite structure reported in Bronsema et al. (1986). The same procedure was also applied to Os in molybdenite, since β-decay without emission of γ-rays, such as the decay of ^{187}Re to ^{187}Os (energy of β-ray: 2.6 keV; Parrington et al., 1996), is not accompanied by a large average recoil that can rupture the bonds of solid matrices (e.g., Maddock et al., 1992). Therefore, Os most likely remains in the same site as Re in molybdenite after the decay. The validity of this assumption for the EXAFS simulation is further discussed in Section 4. For the analysis of ReS_2 and OsS_2 spectra, the initial structure data to run FEFF were obtained from their crystallographic data in Murray et al. (1994) and Stingl et al. (1992), respectively.

After background subtraction from the observed spectra and normalization, the smooth Re or Os L_{III}-edge absorption of the free atom was removed using a cubic spline curve. The energy unit was transformed from keV to $Å^{-1}$ to produce the EXAFS function $\chi(k)$, where k ($Å^{-1}$) is the photoelectron wave vector given by $\sqrt{2m(E-E_0/h^2)}$ (E: the energy of the incident X-ray; E_0: the threshold energy). The E_0 value was determined from the maximum value in the first derivative of $\chi(k)$ in the absorption edge region. The k^3-weighted $\chi(k)$ function was Fourier transformed from k (1/Å) space into R (Å) space to give a radial structural function (RSF). The theoretical EXAFS function was fitted to the back transformed k^3-weighted $\chi(k)$ functions using parameters generated by FEFF 7.02. During the simulation, it was found that multiple scattering is not important in all systems examined in this study. The EXAFS analysis gives the coordination number (CN), the interatomic distance between absorber and scatterer atoms (R), the Debye–Waller term (σ^2), and the energy offset (ΔE_0). The S_0^2 (dumping factor) was fixed at unity in our simulation. The maximum number of parameters for EXAFS fittings was restricted below N_{free} defined as $N_{free}=\frac{2\Delta k\cdot\Delta r}{\pi}+2$ (Stern, 1993), where Δk and Δr are k region (1/Å) of Fourier transformation and R region (Å) of back Fourier transformation, respectively.

3. RESULTS

3.1. Characterization of the Onganja molybdenite

The age of the Onganja molybdenite is calculated to be 505 ± 6 Ma, assuming that all Os is a decay product of ^{187}Re. The uncertainty in the age includes that of the decay constant, $\lambda = (1.666 \pm 0.017) \times 10^{-11}$ years^{-1} (Smoliar et al., 1996). This is in accordance with the Re–Os age of 510 ± 40 Ma for molybdenite in the Onganja Mine reported by Schieder et al. (1981) (recalculated using $\lambda = 1.666 \times 10^{-11}$ years^{-1}), and also with the K–Ar age of 480 ± 25 Ma for a biotite in the molybdenite-bearing vein (Clifford, 1967). Similar Re–Os and K–Ar ages suggest that the Re–Os and K–Ar isotope systems were not disturbed by later hydrothermal or magmatic activity.

3.2. Rhenium L_{III}-edge XAFS of Onganja molybdenite

Rhenium L_{III}-edge XANES spectra of reference materials and Re in the molybdenite are shown in Fig. 1. The molybdenite sample shows a peak of XANES close to those of $Re^{IV}S_2$ and Re metal. Its shoulder at about 10.534 keV is similar to that of ReS_2, but dissimilar to that of Re metal. In addition, the intensity of the "white line" (= main peak in the XANES spectrum) of Re in molybdenite is similar to that of ReS_2. These results suggest that the local atomic environment of Re in molybdenite is similar to that of ReS_2 and that the oxidation state of Re in molybdenite is Re(IV), as suggested in previous studies (Fleischer, 1959; Newberry, 1979; Stein et al., 2001). The results confirm that Mo(IV) in molybdenite can be readily substituted for by Re(IV).

The EXAFS data suggest that local structures of Re in molybdenite and ReS_2 are similar to that of Mo in molybdenite (Figs. 2 and 3). The k^3-weighted Re L_{III}-edge EXAFS spectra $\chi(k)$ and the radial structural function (RSF) obtained by Fourier transforms from k^3-weighted $\chi(k)$ were simulated by the parameters generated by FEFF 7.02. The structure for the FEFF calculation was created based on the molybdenite structure, assuming that Re is in the Mo site. In the EXAFS simulation of Re in molybdenite, the coordination numbers (CN) of S and Mo were fixed at 6 based on the crystallographic information. In the k^3 $\chi(k)$ pattern, the EXAFS oscillation for Re in the molybdenite sample is similar to Re in ReS_2 at k below 6 $Å^{-1}$, since a similar Re–S shell is mainly responsible for the oscillation in the k region (Fig. 2a). However, the oscillation patterns for Re in molybdenite and ReS_2 become different in the larger k region, suggesting that the second neighboring atoms for the two are different. The parameters obtained by the simulation are tabulated in Table 1. In the molybdenite sample, the distance between Re and S is 2.389 Å (Table 1), which is similar to the distance, 2.401 Å, between Mo and S in molybdenite (polytype 2H), based on crystallographic studies (Table 1). The interatomic distance of the second shell, Re–Mo, in the molybdenite sample was calculated to be 3.157 Å, which is also very close to the Mo–Mo distance (3.154 Å) in molybdenite in the literature (Hassel, 1925; Kalikhman, 1983; Schoenfeld et al., 1983; Bronsema

Table 1
EXAFS analyses results obtained by the simulation using parameters generated by FEFF 7.02

Sample	Edge	Analyzed shells	Shell	CN	R (Å)	ΔE_0 (eV)	σ^2 ($\times 10^3$)	N_{free}	Literature values			
									Compounds	Shell	CN	R (Å)
ReS_2	Re L_{III}	2 shells	Re–S	5.9 ± 0.3	2.388 ± 0.003	6.0 ± 0.5	6.1 ± 0.04	12	ReS_2	Re–S	6	2.312–2.504[c]
			Re–Re	3.0[a]	2.777 ± 0.007	—	7.1 ± 0.01			Re–Re	3	2.790–2.896[d]
Molybdenite	Re L_{III}	2 shells	Re–S	6.0[a]	2.389 ± 0.002	6.8 ± 0.4	0.44 ± 0.04	13	MoS_2	Mo–S	6	2.401 ± 0.026[e]
			Re–Mo	6.0[a]	3.157 ± 0.018	—	5.3 ± 0.01			Mo–Mo	6	3.154 ± 0.010[e]
OsS_2	Os L_{III}	3 shells	Os–S	5.7 ± 0.1	2.353 ± 0.001	8.6 ± 0.3	0.63 ± 0.04	18	OsS_2	Os–S	6	2.352 ± 0.001[f]
			Os–S	6.0[a]	3.556 ± 0.007	—	2.8 ± 0.04			Os–S	6	3.565 ± 0.001[f]
			Os–Os	12.0[a]	3.974 ± 0.001	—	2.5 ± 0.12			Os–Os	12	3.974[f]
Molybdenite	Os L_{III}	1 shell[b]	Os–S	6.0[a]	2.271 ± 0.022	-2.9 ± 3.5	0.40 ± 5.3	6				
Molybdenite	Os L_{III}	2 shells[b]	Os–S	6.0[a]	2.272 ± 0.021	-5.1 ± 0.2	0.23 ± 8.3	8				
			Os–Mo	6.0[a]	3.18 ± 0.41	—	1.2 ± 0.01					

Corresponding literature values were also listed. CN, coordination number; R, interatomic distance; ΔE_0, threshold E_0 shift; σ, Debye–Waller term; N_{free}, maximum number of parameters. Least squares precisions are given to each value.

[*] Errors in the fitted parameters were estimated to be generally ± 0.02 Å for R, $\pm 20\%$ for N, and 20% for σ^2 (O'Day et al., 1994).

[a] Fixed in the simulation.

[b] For Os in the molybdenite sample, two simulations were performed; one considers only the first shell and the other the first and second shells in RSF.

[c] In ReS_2, the distances between Re and neighboring six S atoms are different (Murray et al., 1994).

[d] In ReS_2, the distances between Re and neighboring three Re atoms are different (Murray et al., 1994).

[e] Average and 1σ of four reported values (Hassel, 1925; Kalikhman, 1983; Schoenfeld et al., 1983; Bronsema et al., 1986).

[f] Average and 1σ of 2 reported values (Knop and Reid, 1967; Stingl et al., 1992). Two reported values were idential for the Os–Os.

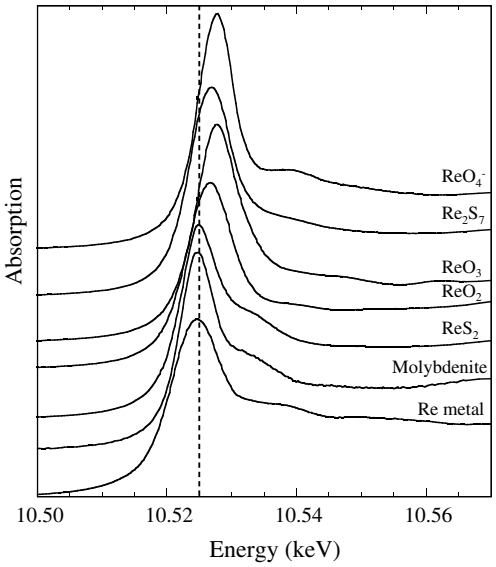

Fig. 1. Rhenium L_{III}-edge XANES for Re in molybdenite and Re reference materials such as Re metal, $Re^{IV}S_2$, $Re^{IV}O_2$, $Re^{VI}O_3$, $Re^{VII}{}_2S_7$, and $Re^{VII}O_4^-$ in aqueous solution.

et al., 1986). These results clearly show that Re resides in the Mo site of molybdenite.

Rhenium in ReS_2 was also examined by EXAFS (Fig. 3). The CN of Re–S was optimized by the simulation, while CN for the second shell, Re–Re, was fixed at 3 as discussed in Murray et al. (1994). The interatomic distance and the CN of the first shell, Re–S, were calculated to be 2.388 Å and 5.9, respectively (Table 1). Although the crystallographic data of ReS_2 suggest different distances between Re and six S, our EXAFS and XANES data showed that the local atomic environment of Re in molybdenite is very similar to that of ReS_2, which allows a significant substitution of Mo by Re in molybdenite, as previously noted by many workers (e.g., Fleischer, 1959; Terada et al., 1971; Stein et al., 2001).

It has been suggested that Re may form its own phase, ReS_2 in molybdenite (Newberry, 1979). However, this possibility is discounted because the position of the second peak in RSF is different between Re in molybdenite and ReS_2. In addition, the amplitude of the $k^3\chi(k)$ function at k around 7 $Å^{-1}$ and the oscillation period of EXAFS are clearly different between Re in molybdenite and ReS_2, which can be explained by contributions of Re–Mo in

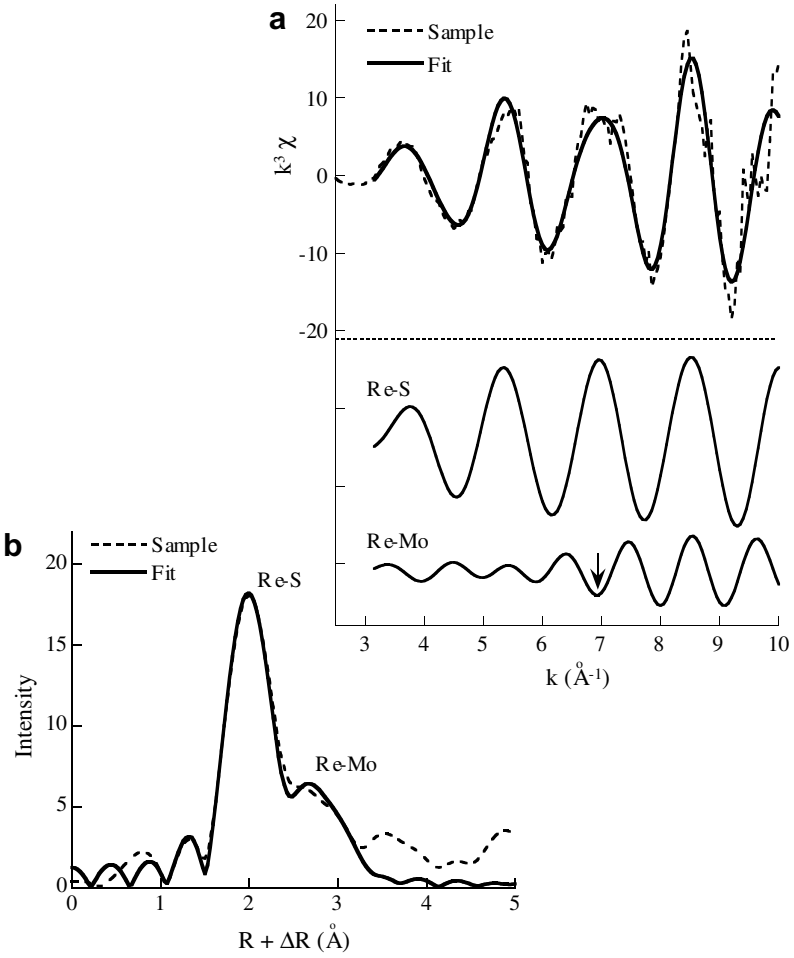

Fig. 2. EXAFS results for Re in molybdenite including (a) k^3-weighted Re L_{III}-edge EXAFS spectra $\chi(k)$ with the simulated spectrum, including the contribution of the first shell (Re–S) and second shell (Re–Mo) and (b) Radial structure functions obtained by Fourier transforms from k^3-weighted $\chi(k)$ for Re with the simulation curve; an arrow shows the contribution of the Re–Mo shell at around 7 Å, which is different from that of the Re–Re shell in Fig. 3.

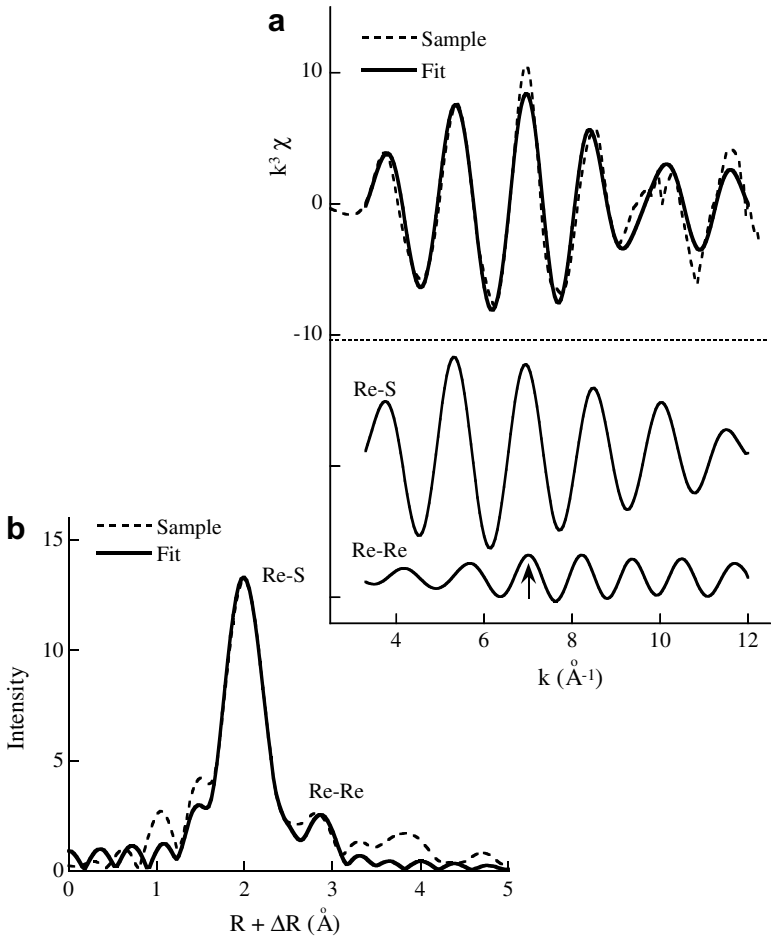

Fig. 3. EXAFS results for Re in ReS_2 including (a) k^3-weighted $\chi(k)$ with the simulated spectrum with the contribution of Re–S and Re–Re shells considered in the simulation and (b) RSF for Re with the simulation curve; an arrow at around 7 Å shows the contribution of Re–Re shell.

molybdenite and Re–Re in ReS_2 (arrows in Figs. 2a and 3a). The simulation of the EXAFS, assuming Re as the second neighboring atom in molybdenite, yielded a Re–Re interactomic distance of 3.06 Å. This distance is impossibly longer than the interatomic distance of Re–Re in ReS_2, 2.77 Å (Table 1). These results confirm that Re does not form its own phase, ReS_2, in molybdenite.

3.3. Fluorescence XAFS at Os L_{III}-edge using a crystal analyzer

It was impossible to record Os L_{III}-edge XAFS for radiogenic Os in the molybdenite by normal fluorescence mode with SSD, since intense fluorescence X-rays from Re and other elements conceal a small Os L_α peak (Fig. 4). In addition, large scattering X-rays around 11 keV and fluorescence X-rays below 7.2 keV (mainly from Fe) saturates SSD counting, which makes the detection of a small Os L_α peak impossible. The use of a crystal analyzer placed between the sample and the detector allowed us to extract the Os L_α peak. Since some interferences on Os L_α fluorescence from Re was still found in the XRF spectrum even with the use of the analyzer, the quality of XAFS spectra of Os was further improved by the use of a Ge semiconductor detector coupled with the crystal analyzer system.

3.4. Osmium L_{III}-edge XAFS of Onganja molybdenite

Osmium L_{III}-edge XANES for Os in molybdenite were successfully measured by the fluorescence mode using the crystal analyzer system (Fig. 5). The main peak of Os in molybdenite is close to those for Os metal and OsS_2, whereas a shoulder of about 10.877 keV is present both for OsS_2 and Os in molybdenite. However, the intensity of the main peak for Os in molybdenite is clearly larger than those of Os metal and OsS_2 (Fig. 5). It is known from the studies of platinum group elements that the intensity of the main peak of the electron transition from 2p to 5d is proportional to the hole of the 5d electron orbitals, or the oxidation state (Lytle et al., 1979; Sinfelt et al., 1981; Mansour et al., 1984; Santiago et al., 2003; Rhee et al., 2003). This is confirmed by a linear positive correlation between the main peak intensity and the oxidation state of Os for the reference materials in this study (Fig. 6). The intensity

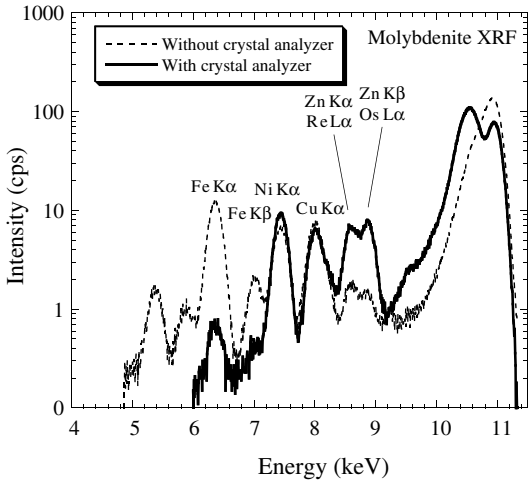

Fig. 4. X-ray fluorescence spectra of Onganja molybdenite irradiated at 11 keV with (solid line) and without (dashed line) crystal analyzer system.

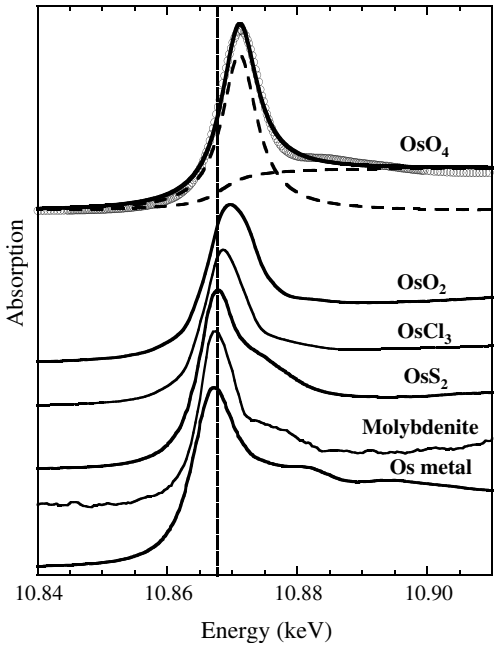

Fig. 5. Osmium L_{III}-edge XANES for Os in molybdenite and reference materials including Os metal, $Os^{II}S_2$, $Os^{III}Cl_3$, $Os^{IV}O_2$, and $Os^{VIII}O_4$. The simulation of the "white line" is shown for OsO_4 where the results in bold combine the Lorentzian and arctangent functions (both in broken curves). The measured values, shown as open circles, are similar to the simulated results, confirming the validity of the latter.

was obtained as the area of the Lorentzian function, which was used to simulate XANES spectrum with the combination of arc-tangent function. In the simulation, the relative position of Lorentzian and arc-tangent functions were fixed as constant (Takahashi et al., 2005). The simulation for OsO_4 is shown as an example in Fig. 5. The linear relation and the area of Lorentzian function in the XANES spectrum suggest that the average oxidation state of Os in molybdenite is 3.6 ± 0.1, i.e., a mixture of Os(III) and Os(IV). This result is unexpected, since Os is divalent in natural sulfides and arsenides, such as erlichmanite ($Os^{II}S_2$), anduoite ($Os^{II}As_2$), and ruarsite $(Ru,Os)^{II}AsS$. The presence of Os at a higher oxidation state is possibly due to the oxidation state of the parent, Re(IV), in molybdenite. The β-decay of Re(IV), which is accompanied by the emission of an electron, may result in the formation of Os(V). The observed oxidation state of Os suggests that Os recaptures electrons to form Os(IV), as suggested by Stein et al. (2003). In addition, electrons may freely move within electrically conductive molybdenite (Macintyre, 1992), which allows further reduction of Os(IV) to Os(III). However, further study is necessary to evaluate the mechanism controlling the oxidation state of radiogenic Os, or more generally the oxidation state of radiogenic isotopes in solid media.

EXAFS results of radiogenic Os in molybdenite and OsS_2 are shown in Figs. 7 and 8, respectively. As shown in the previous section, Re is in the Mo site in molybdenite. It is expected that radiogenic Os remains in the Mo site shortly after decay of ^{187}Re, because β-decay of ^{187}Re would have little radiation effect in the matrices. Thus, the initial structure of Os in the molybdenite to run FEFF calculation was obtained assuming that the Os is at the Mo site in molybdenite. The CNs of the first shell (Os–S) and the second shell (Os–Mo) were fixed at six during the simulation. The simulation was successfully completed yielding the parameters listed in Table 1. The calculated interatomic distance for Os–S is 2.271 Å; a similar value of 2.272 Å is obtained in the simulation that considers only the first shell. The distance is much shorter than those for Mo–S and Re–S (ca. 2.39 Å) in molybdenite, whereas the distance of the

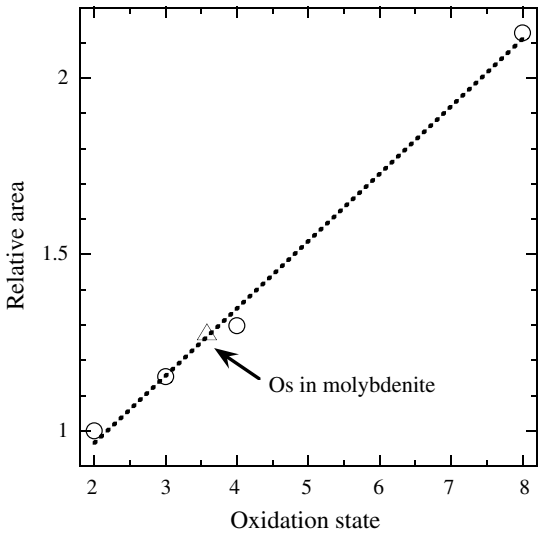

Fig. 6. Relationship between the oxidation state of Os and the area of Lorentzian function simulating the "white line" in Os L_{III}-edge XANES. The simulation was conducted coupling the Lorentzian and arctangent functions as shown in Fig. 5. Circles are data of the reference materials used for the calibration, while the triangle shows the value for Os in molybdenite. The uncertainties of the estimated values are within the symbol size.

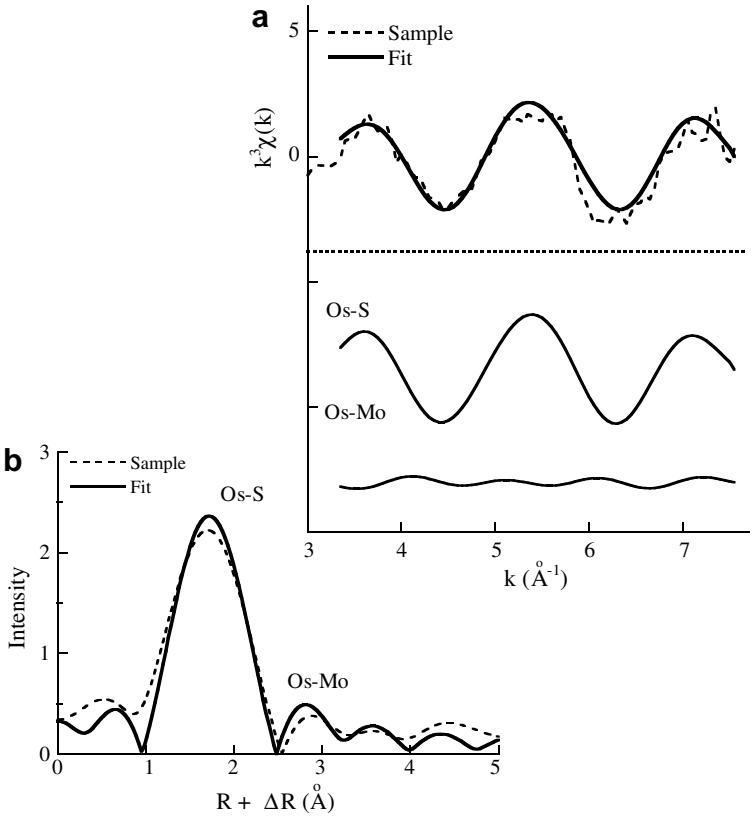

Fig. 7. EXAFS results for Os in molybdenite including (a) k^3-weighted $\chi(k)$ with the simulated spectrum, including contribution of Os–S and Os–Mo shells considered in the simulation. (b) RSF for Os with the simulation curve.

second shell (Os–Mo, 3.18 Å) is similar to those of Re–Mo and Mo–Mo (3.16 Å).

The distance of Os–S in molybdenite is shorter than the distance of Os^{II}–S, 2.35 Å, in erlichmanite (OsS_2), which is explained by the smaller sizes of Os(III) and Os(IV) in molybdenite than Os(II). Within molybdenite, the distance of Os–S is shorter than the distances of Re–S and Mo–S. The shorter distance of Os–S suggests that the presence of Os produces a distortion in the local structure of molybdenite.

4. DISCUSSION

Other Os phases, such as metallic Os and $Os^{II}S_2$, may possibly form as a consequence of the redistribution of Os in molybdenite. However, the EXAFS spectra indicate that Os in molybdenite is not in the metallic form, since the first peak in the RSF is located at about 1.8 Å (phase shift uncorrected), which is much shorter than that of Os metal, 2.2 Å (Sakakibara et al., 2005). The possible formation of OsS_2 in molybdenite is also discounted, since (i) the simulation assuming the structure of OsS_2 (six S atoms were assigned to the first and second shells each; Table 1) did not converge, and (ii) a small peak of OsS_2 at $k = 6.5$ (Å) (Fig. 7) was not found in k^3 $\chi(k)$ spectrum for Os in molybdenite (Fig. 6). These results are also supported by the XANES spectra of OsS_2 and Os metal, which are dissimilar to that of Os in molybdenite, particularly in terms of the magnitude of the "white line" and the position of the shoulder at about 10.87–10.88 keV (Fig. 5).

One may think that the assumption of the initial structure for the EXAFS analysis that Os is at the Re site may not be appropriate when Os has already migrated within the sample. However, no secondary minerals hosting Os, such as Os metal or OsS_2, were identified in the molybdenite of our study. Thus, we conclude that Os is present at the cation site of molybdenite even after Os has migrated in the sample. In the simulation of EXAFS above, we fixed the CN value at 6, but this value can be also determined by the simulation of the EXAFS spectra. As a result of the optimization, it was revealed that the CN value for Os in molybdenite is 6.5 (and Os–S distance is 2.255 Å) in both cases where one-shell and two-shells are considered for the simulation. This confirms that Os is surrounded by six S atoms, as is Mo in MoS_2. Thus, the assumption that Os is at the cation site of molybdenite may be valid.

When MoS_2 is compared to ReS_2 and OsS_2, the interatomic distance and the oxidation state of Re in ReS_2 are identical to Mo in molybdenite, but they are different from Os in OsS_2 (Table 1). In addition, S forms dianion S_2^{2-} in cubic OsS_2 and S^{2-} in hexagonal molybdenite and triclinic ReS_2. Hence, the chemical environment of Re in molybdenite is almost identical to that of Re in ReS_2, whereas the chemical state of Os in molybdenite is not similar to that of Os in OsS_2. The atomic-level environments of Re and

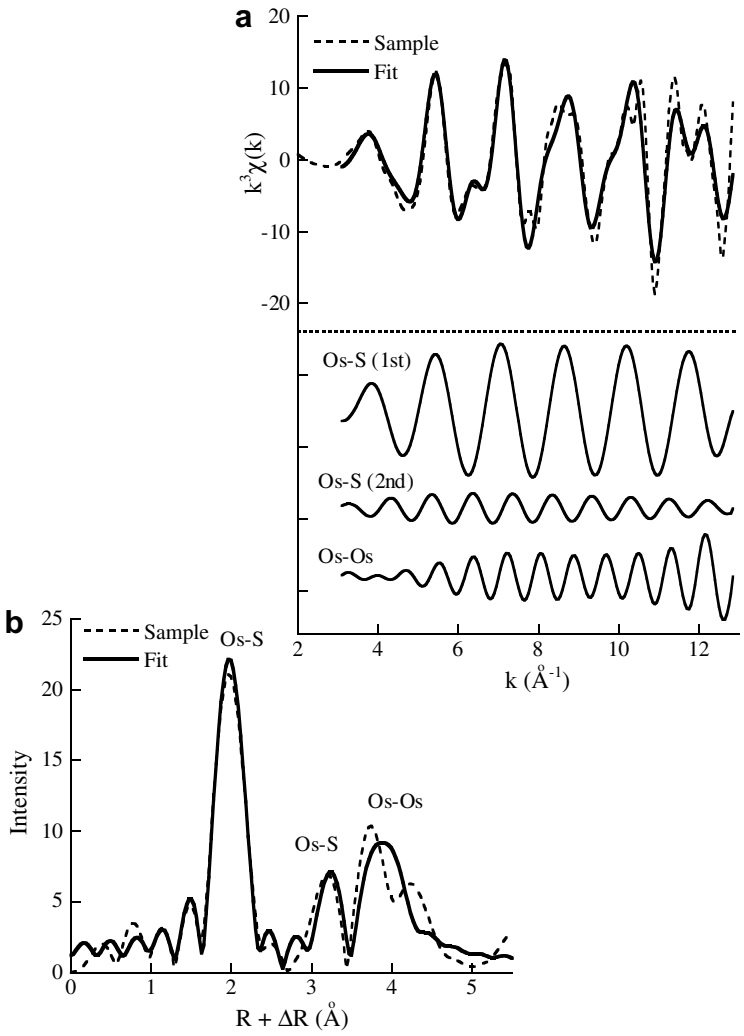

Fig. 8. EXAFS results for Os in OsS_2 including (a) k^3-weighted $\chi(k)$ with the simulated spectrum, including the contribution of two Os–S shells and Os–Os shell considered in the simulation. (b) RSF for Os with the simulation curve.

Os explain the much larger initial abundance of Re than Os in molybdenite. Although the high Re/Os ratio at the time of the mineral formation was already suggested in previous studies (e.g., Morgan et al., 1968; Stein et al., 2001), the fact was supported here by the EXAFS analyses at the atomic level. As a result, molybdenite has been utilized as a suitable mineral for the Re–Os dating.

It has been suggested that radiogenic Os may be mobile in molybdenite, which causes the decoupling of Re–^{187}Os (Stein et al., 2001, 2003; Kosler et al., 2003; Selby and Creaser, 2004). Our data show that radiogenic Os is smaller than Re and that the oxidation state of Os, trivalent or tetravalent, is equal to or smaller than that of Re(IV) in molybdenite. These results suggest that the decoupling is caused by the faster diffusion of radiogenic Os relative to Re in molybdenite, since a smaller cation with lesser charge diffuses faster than a larger one with greater charge (e.g., Cherniak, 1997; Van Orman et al., 2001; Cherniak, 2003). In addition, accumulation of radiogenic Os in defects in molybdenite also suggested in these studies (Stein et al., 2001, 2003; Selby and Creaser, 2004) is compatible with this diffusion model for the Re–^{187}Os decoupling, since ions in crystals tend to diffuse toward defects present in the crystal (e.g., Watson and Baxter, 2007).

As shown in the parabolic relationship between ionic radii and partition coefficients of trace elements in minerals (Onuma et al., 1968), the partition coefficients of larger and smaller ions than the size of a cation at a given site are smaller than for the ion in the site. This relationship shows that crystal structure provides a certain size for each site and smaller or larger ions are not well accommodated into the site. Hence, Os does not physically fit as well as Re in the Mo site of molybdenite and the presence of Os likely creates a minor distortion in the local crystal structure of MoS_2. Structural integrity plays an important role in diffusivity of elements in the crystal with diffusivities of elements being faster around distorted crystals (e.g., Watson and Baxter, 2007). Consequently, Re–^{187}Os ratios may be locally modified in an individual crystal (Stein et al., 2003; Kosler et al., 2003; Selby and Creaser, 2004).

It is well established that the ^{187}Re–^{187}Os geochronometer in molybdenite yields reliable ages when using the whole-molybdenite approach instead of a micro-sampling technique, such as a laser ablation technique (Markey et al., 1998; Stein et al., 2001, 2003; Selby and Creaser, 2004; Stein, 2006). Fast diffusion of ^{187}Os may cause the decoupling of Re–^{187}Os in a small area in molybdenite, but the Os may likely remain within the crystal. Our results confirm that that Re–Os ages determined using micro-analytical techniques may not be reliable; dating of whole crystals or aggregates of representative fine grains of molybdenite is recommended.

5. SUMMARY

XAFS spectra were successfully measured for Re and radiogenic ^{187}Os in molybdenite using a crystal analyzer. The XANES and EXAFS results of Re and Os in molybdenite show that (i) Re and radiogenic ^{187}Os reside in the Mo site in molybdenite, (ii) the interatomic distance of Re to neighboring S and the oxidation state of Re in molybdenite are similar to those for Mo in molybdenite and Re in ReS_2, (iii) the interatomic distance of radiogenic ^{187}Os to S is smaller by 0.12 Å than those of Re–S and Mo–S in molybdenite, and (iv) the oxidation state of radiogenic ^{187}Os is Os(III) and Os(IV), similar to Re(IV) and Mo(IV) in molybdenite. These results suggest that the oxidation state of ^{187}Os is related to the parent Re(IV), which induces the shorter interatomic distance of Os^{IV}-S or Os^{III}–S in molybdenite compared to that of Os^{II}–S in erlichmanite. Due to the small size and lower charge, radiogenic ^{187}Os diffuses faster than Re in molybdenite. Our results provide structural chemical evidence for interpreting the geochemical observations reported in other studies; these include (i) the abundance of Os in molybdenite is much less than that of Re, and (ii) Os has a higher mobility than Re, promoting the decoupling of Re and ^{187}Os in molybdenite.

ACKNOWLEDGMENTS

We thank Mrs. M. Fukukawa and Y. Yamamoto for their help in XAFS experiments. Dr. McG. Miller is greatly acknowledged for providing the molybdenite sample. We are grateful to Prof. K. Hayashi (Okayama University of Science) for synthesizing the OsS_2 sample. Finally, we thank an anonymous journal reviewer and Dr. H. Stein (Colorado State University) for their helpful comments, which have greatly improved this paper. This study was supported by a Grant-in-Aid for Scientific Research from the Japan Society for the Promotion of Science and funds from Shimadzu Science Foundation and Nippon Seimei Foundation. This work has been performed with the approval of SPring-8 (Proposal No. 2001B0393, R04A38B1-0023N, 2004B0169, and 2005B0181) and Photon Factory, KEK (Proposal No. 2004G119 and 2004G334).

REFERENCES

Ankudinov A. L. and Rehr J. J. (1997) Relativistic calculations of spin-dependent X-ray absorption spectra. *Phys. Rev.* **B56**, 1712–1716.

Bronsema K. D., de Boer J. L. and Jellinek F. (1986) On the structure of molybdenum diselenide and disulfide. *Zeitschrift für Anorganische und Allgemeine Chemie* **540**, 15–17.

Cherniak D. J. (1997) Rare-earth diffusion in zircon. *Chem. Geol.* **134**, 289–301.

Cherniak D. J. (2003) REE diffusion in feldspar. *Chem. Geol.* **193**, 25–41.

Clifford T. N. (1967) The Damaran Episode in the Upper Proterozoic-Lower Paleozoic structural history of Southern Africa. *Spec. Pap. Geol. Soc. Am.* **92**, 100.

Faure G. and Mensing T. M. (2004) *Isotopes: Principles and Applications*. Wiley, New York.

Fleischer M. (1959) The geochemistry of rhenium, with special reference to its occurrence in molybdenite. *Econ. Geol.* **54**, 1406–1413.

Hassel O. (1925) Ueber die Kristallstruktur des Molybdaenglanzes. *Zeitschrift fuer Kristallographie, Kristallgeometrie, Kristallphysik, Kristallchemie* **61**, 92–99.

Hayashi K., Serikawa D., Maeda N., Okamoto A. and Ikeuchi T. (2000) Microwave absorption materials-IV Preparation of the mixed layer structure phases, $Re_xTa_{1-x}S_2$ and $Os_xTa_{1-x}S_2$, and some electrical and magnetic properties. *J. Eur. Ceram. Soc.* **20**, 2735–2742.

Herr W. and Merz E. (1955) Eine neue Methode zur Alterbestimmung von rhenium-haltigen mineralien mittels neutronaktivierung. *Z. Naturforsch.* **10a**, 613–615.

Hirt B., Herr W. and Hoffmeister W. (1963) Age determinations by the rhenium–osmium method. In *Radioactive Dating*. International Atomic Energy Agency, Vienna, pp. 35–43.

Kalikhman V. L. (1983) Characteristics of the crystal structure, electrophysical properties, and model of the valence band spectrum of laminar compounds of molybdenum disulfide type. *Acta Crystallogr. B* **39**, 404–407.

Knop O. and Reid K. I. G. (1967) Chalcogenides of the transition elements. V. Crystal structures of the disulfides and ditellurides of ruthenium and osmium. *Can. J. Chem.* **45**, 1391–1400.

Kosler J., Simonetti A., Sylvester P., Cox R., Tubrett M. N. and Wilton D. (2003) Laser ablation ICP-MS measurements of Re/Os in molybdenites and implications for Re–Os geochronology. *Can. Mineral.* **41**, 307–320.

Lytle F. W., Wei P. S. P., Greegor R. B., Via G. H. and Sinfelt J. H. (1979) Effect of chemical environment on magnitude of X-ray absorption resonance at L_{III} edges. Studies on metallic elements, compounds, and catalysts. *J. Chem. Phys.* **70**, 4849–4855.

Maddock A. G., Sakanoue M., Willard J. E. and Hoffma D. C. (1992) Historical development of hot atom chemistry and prospects. In *Handbook of Hot Atom Chemistry* (eds. J.-P. Adloff, P. P. Gaspar, M. Imamura, A. G. Maddock, T. Matsuura, H. Sano and K. Yoshihara). VCH, Tokyo, pp. 3–31.

Mansour A. N., Cook J. W. and Sayers D. E. (1984) Quantitative technique for the determination of the number of unoccupied d-electron states in a platinum catalyst using the $L_{2,3}$ X-ray absorption-edge spectra. *J. Phys. Chem.* **88**, 2330–2334.

Markey R., Stein H. and Morgan J. (1998) Highly precise Re–Os dating for molybdenite using alkaline fusion and NTIMS. *Talanta* **45**, 935–946.

Macintyre, J. E. (ed.) (1992) Dictionary of Inorganic Compounds, vol. 3. Chapman & Hall, London, pp. 3594.

Morgan J. W., Lovering J. F. and Ford R. J. (1968) Rhenium and non-radiogenic osmium in Australian molybdenites and other sulphide minerals by neutron activation analysis. *J. Geol. Soc. Aust.* **15**, 189–194.

Murray H. H., Kelty S. P., Chianelli R. R. and Day C. S. (1994) Structure of rhenium disulfide. *Inorg. Chem.* **33**, 4418–4420.

Newberry R. J. J. (1979) Polytypism in molybdenite (II): relationships between polytypism, ore deposition/alteration stages and rhenium contents. *Am. Mineral.* **64**, 768–775.

Nomura M. (1998) Dead-time correction of a multi-element SSD for fluorescent XAFS. *J. Synchrotron Rad.* **5**, 851–853.

Nomura M. and Koyama A. (1996) Design and performance of a new XAFS beamline at the photon factory; BL-12C. *KEK Rep.*, 15–95.

O'Day P. A., Rehr J. J., Zabinsky S. I. and Brown G. E. (1994) Extended X-ray absorption fine structure (EXAFS) analysis of disorder and multiple scattering in complex crystalline solids. *J. Am. Chem. Soc.* **116**, 2938–2949.

Onuma N., Higuchi H., Wakita H. and Nagasawa H. (1968) Trace elements partition between two pyroxenes and the host lava. *Earth Planet. Sci. Lett.* **5**, 47–51.

Parrington J. R., Knox H. D., Breneman S. L., Baum E. M. and Feiner F. (1996) *Nuclides and Isotopes*, 15th ed. GE Nuclear Energy, San Jose.

Raith J. G. and Stein H. J. (2000) Re–Os dating and sulfur isotope composition of molybdenite from tungsten deposits in western Namaqualand, South Africa: implications for ore genesis and the timing of metamorphism. *Mineral. Dep.* **35**, 741–753.

Ravel B. (2001) ATOMS: crystallography for the X-ray absorption spectroscopy. *J. Synchrotron Rad.* **8**, 314–316.

Rhee C. K., Wakisaka M., Tolmachev Y. V., Johnston C. M., Haasch R., Attenkofer K., Lu G. Q., You H. and Wieckowski A. (2003) Osmium nanoislands spontaneously deposited on a Pt(111) electrode: an XPS, STM and GIF-XAS study. *J. Electroanal. Chem.* **554**, 367–378.

Sakakibara N., Takahashi Y., Okumura K., Hattori K. H., Yaita T., Suzuki K. and Shimizu H. (2005) Speciation of osmium in an iron meteorite and a platinum ore specimen based on X-ray absorption fine-structure spectroscopy. *Geochem. J.* **39**, 383–389.

Santiago E. I., Giz M. J. and Ticianelli E. A. (2003) Studies of carbon monoxide oxidation on carbon-supported platinum–osmium electrocatalysts. *J. Solid State Electrochem.* **7**, 607–613.

Schieder R., Sorgalla K. H. and Herr W. (1981) The determination of osmium isotope abundances by high resolution laser spectroscopy. *Radiochim. Acta* **28**, 109–113.

Selby D. and Creaser R. A. (2001a) Re–Os geochronology and systematics in molybdenite from the Endako porphyry molybdenum deposit, British Columbia, Canada. *Econ. Geol.* **96**, 197–204.

Selby D. and Creaser R. A. (2001b) Late and mid-Cretaceous mineralization in the Northern Canadian Cordillera: constraints from Re–Os molybdenite dates. *Econ. Geol.* **96**, 1461–1467.

Selby D. and Creaser R. A. (2004) Macroscale NTIMS and microscale LA-MC-ICP-MS Re–Os isotopic analysis of molybdenite: testing spatial restrictions for reliable Re–Os age determinations, and implications for the decoupling of Re and Os within molybdenite. *Geochim. Cosmochim. Acta* **68**, 3897–3908.

Schoenfeld B., Huang J. J. and Moss S. C. (1983) Anisotropic mean-square displacement (MSD) in single crystals of 2H- and 3R-MoS_2. *Acta Crystallogr. B* **39**, 404–407.

Sinfelt J. H., Via G. H., Lytle F. W. and Greegore R. B. (1981) Structure of bimetallic clusters. Extended X-ray absorption fine-structure (EXAFS) studies of Os–Cu clusters. *J. Chem. Phys.* **75**, 5527–5537.

Smoliar M. L., Walker R. J. and Morgan J. W. (1996) Re–Os ages of group IIA, IIIA, IVA, and IVB iron meteorites. *Science* **271**, 1099–1102.

Stein H. J. (2006) Low-rhenium molybdenite by metamorphism in northern Sweden: recognition, genesis, and global implications. *Lithos* **87**, 300–327.

Stein H. J., Markey R. J., Morgan J. W., Du A. and Sun Y. (1997) Highly precise and accurate Re–Os ages for molybdenite from the East Qinling molybdenum belt, Shaanxi Province, China. *Econ. Geol.* **92**, 827–835.

Stein H. J., Sundblad K., Morgan J. W., Markey R. J. and Motuza G. (1998) Re–Os ages for Archean molybdenite and pyrite, Kuittila, Finland and Proterozoic, Kabeliai, Luthuania: a metamorphic and metasomatic test for the chronometer. *Mineral. Dep.* **33**, 329–345.

Stein H. J., Markey R. J., Morgan J. W., Hannah J. L. and Scherste'n A. (2001) The remarkable Re–Os chronometer in molybdenite: how and why it works. *Terra Nova* **13**, 479–486.

Stein H., Scherst'en A., Hannah J. and Markey R. (2003) Subgrain-scale decoupling of Re and ^{187}Os and assessment of laser ablation ICP-MS spot dating in molybdenite. *Geochim. Cosmochim. Acta* **67**, 3673–3686.

Stingl T., Mueller B. and Lutz H. D. (1992) Crystal structure refinement of osmium(II) disulfide. *Zeitschrift fuer Kristallographie* **202**, 161–162.

Stern E. A. (1993) Number of relevant independent points in X-ray absorption fine-structure spectra. *Phys. Rev.* **B48**, 9825–9827.

Suzuki K., Qilu Shimizu H. and Masuda A. (1992) Determination of osmium abundance in molybdenite mineral by isotope-dilution mass-spectrometry with microwave digestion using potassium dichromate as oxidizing-agent. *Analyst* **117**, 1151–1156.

Suzuki K., Shimizu H. and Masuda A. (1996) Re–Os dating of molybdenites from ore deposits in Japan: implications for the closure temperature of the Re–Os system for molybdenite and the cooling history of molybdenum ore deposits. *Geochim. Cosmochim. Acta* **60**, 3151–3159.

Takahashi Y., Shimizu H., Usui A., Kagi H. and Nomura M. (2000) Direct observation of tetravalent cerium in ferromanganese nodules and crusts by X-ray absorption near-edge structure (XANES). *Geochim. Cosmochim. Acta* **64**, 2929–2935.

Takahashi Y., Minamikawa R., Hattori H. K., Kurishima K., Kihou N. and Yuita K. (2004) Arsenic behavior in paddy fields during the cycle of flooded and non-flooded periods. *Environ. Sci. Technol.* **38**, 1038–1044.

Takahashi Y., Kolonin G. R., Shironosova G. P., Kupriyanova I. I., Uruga T. and Shimizu H. (2005) Determination of the Eu(II)/Eu(III) ratios in minerals by X-ray absorption near-edge structure (XANES) and its application to hydrothermal deposits. *Min. Mag.* **69**, 177–188.

Takahashi Y., Uruga T., Tanida H., Terada Y., Nakai S. and Shimizu H. (2006) Application of X-ray absorption near-edge structure (XANES) using bent crystal analyzer to the speciation of trace Os in iron meteorites. *Anal. Chim. Acta* **558**, 332–336.

Terada K., Osaki S., Ishihara S. and Kiba T. (1971) Distribution of rhenium in molybdenites. *Geochem. J.* **4**, 123–141.

Terada Y., Goto S., Takimoto N., Takeshita K., Yamazaki H., Shimizu Y., Takahashi S., Ohashi H., Furukawa Y., Matsushita T., Ohata T., Ishizawa Y., Uruga T., Kitamura H., Ishikawa T. and Hayakawa S. (2004) Construction and Commissioning of BL37XU at SPring-8. *AIP Conf. Proc.* **705**, 376–379.

Van Orman J. A., Grove T. L. and Shimizu N. (2001) Rare earth element diffusion in diopside: influence of temperature, pressure, and ionic radius, and an elastic model for diffusion in silicates. *Contrib. Mineral. Petrol.* **141**, 687–703.

Watanabe Y. and Stein H. J. (2000) Re–Os ages for the Erdenet and Tsagaan Suvarga porphyry Cu–Mo deposits, Mongolia, and tectonic implications. *Econ. Geol.* **95**, 1537–1542.

Watson E. B. and Baxter E. F. (2007) Diffusion in solid-Earth systems. *Earth Planet. Sci. Lett.* **253**, 307–327.

Zavinsky S. I., Rehr J. J., Ankudinov A., Albers R. C. and Eller M. J. (1995) Multiple scattering calculations of X-ray absorption spectra. *Phys. Rev.* **B52**, 2995–3009.

Zhong Z., Chapman D., Bunker B., Bunker G., Fischetti R. and Segre C. (1999) A bent Laue analyzer for fluorescence EXAFS detection. *J. Synchrotron Rad.* **6**, 212–214.

Associate editor: Edward M. Ripley